How to cite: *Angew. Chem. Int. Ed.* **2024**, *63*, e202318872
doi.org/10.1002/anie.202318872

VIP Oxygen Reduction Very Important Paper

Synergistic Ni–W Dimer Sites Induced Stable Compressive Strain for Boosting the Performance of Pt as Electrocatalyst for the Oxygen Reduction Reaction

Xiaozhang Yao[+], Zhongxin Song[+], Xue Yao[+], Yi Guan, Natalie Hamada, Jingyan Zhang, Ziwei Huo, Lei Zhang, Chandra Veer Singh,* and Xueliang Sun**

Abstract: Alloying Pt catalysts with transition metal elements is an effective pathway to enhance the performance of oxygen reduction reaction (ORR), but often accompanied with severe metal dissolution issue, resulting in poor stability of alloy catalysts. Here, instead of forming traditional alloy structure, we modify Pt surface with a novel Ni–W dimer structure by the atomic layer deposition (ALD) technique. The obtained NiW@PtC catalyst exhibits superior ORR performance both in liquid half-cell and practical fuel cell compared with initial Pt/C. It is discovered that strong synergistic Ni–W dimer structure arising from short atomic distance induced a stable compressive strain on the Pt surface, thus boosting Pt catalytic performance. This surface modification by synergistic dimer sites offers an effective strategy in tailoring Pt with excellent activity and stability, which provides a significant perspective in boosting the performance of commercial Pt catalyst modified with polymetallic atom sites.

[*] X. Yao,[+] Y. Guan, J. Zhang, Z. Huo, X. Sun
Department of Mechanical and Materials Engineering, University of Western Ontario, London, ON, N6 A 5B9, Canada
E-mail: xsun9@uwo.ca

X. Sun
Eastern Institute for Advanced Study, Eastern Institute of Technology, Ningbo, Zhejiang 3150200, China

Z. Song,[+] L. Zhang
College of Chemistry and Environmental Engineering, Shenzhen University, Shenzhen 518071, China
E-mail: lei.zhang@szu.edu.cn

X. Yao,[+] C. V. Singh
Department of Materials Science and Engineering, University of Toronto, Toronto, ON, M5S 3E4, Canada
E-mail: chandraveer.singh@utoronto.ca

N. Hamada
Canadian Centre for Electron Microscopy, Hamilton, ON, L8S 4M1, Canada

[+] These authors contributed equally.

Introduction

The sluggish oxygen reduction reaction(ORR) is one of the main bottleneck in the commercial application of proton exchange membrane fuel cells.[1] Platinum(Pt) electrocatalysts have been considered as a universal choice to accelerate the ORR, but the high cost and subpar performance of Pt present significant challenges.[2] Alloying with transition metal (e.g. Fe, Co, Ni, etc.) has been proven to be an efficient approach to accelerate the ORR activity, particularly PtNi alloy was demonstrated to be one of most active catalysts, owing to its specific composition and strain effects.[3] However, the non-noble metal suffers from continuous leaching during long term ORR tests, leading to weak strain effects and thus dramatic activity degradation.[2c,4] Recently, rather than forming alloy structure, modifying Pt surface with single atom has emerged as a promising approach.[5] Theoretically, this approach capitalizes on the remarkable enhancement of catalytic activity or stability through single atom modification effects. For instance, Co single atom decorated Pt nanoparticle supported on nitrogen doped carbon nanotube exhibited greatly enhanced mass activity compared with undoped Pt catalysts, although it did not address durability concern.[5b] Therefore, achieving Pt electrocatalysts with excellent activity and stability simultaneously for practical fuel cells application is significantly necessary.

Due to the simplicity of single atom structure, further tuning coordination structure with secondary element to forming dimer atoms structure would be promising to boost catalytic performance because of the bimetallic functional sites and synergistic effects.[6] For instance, Fe–Co, Zn–Co, Ni–Fe dimer active sites have been elucidated as efficient electrocatalysts in ORR and other electrocatalytic reactions.[5d,7] Thus, rationally designing dimer atoms modification for Pt electrocatalysts with superior ORR performance in terms of activity and stability concurrently is quite appealing. However, the main challenge lies in precisely controlling the location of each atomic sites, especially synthesizing A–B bimetallic dimer sites to achieving strong synergistic effects. Among the various preparation methods, the atomic layer deposition (ALD) method is a powerful technique to build atom to atom pairs and even multiple atoms, owing to the self-limiting and selectivity.[8] For example, bimetallic Pt–Ru dimer electrocatalysts with exceptional activity for hydrogen evolution reaction was

successfully prepared by ALD method.[6b] Thus, through deliberate design, ALD offers a prospective pathway to forming A–B dimer sites on the metal surface. Furthermore, deep insight into the role of dimer structure on the metal surface have yet to be fully explored, especially emphasizing the strain effects.

Regarding the element selection of A–B dimer sites, element pairs with stability and activity enhancement effects for Pt were considered. In this case, we chose tungsten (W) and nickel (Ni) atoms to modify Pt catalysts. W element is widely used in alloy electrocatalysts to enhance stability due to its strong acid-resistant property and stable structure.[9] PtNi alloy electrocatalysts have been proven as one of the most effective ORR catalysts.[3a,10] Therefore, the incorporation of W species with Ni elements to form a synergistic dimer structure is expected to improve both activity and stability of Pt electrocatalysts for the ORR. Herein, Ni–W dimer sites modified Pt nanoparticles with nearly full exposed Pt surface were successfully prepared by ALD process. The detailed structure of Ni–W dimer sites was investigated using high-angle annular dark field scanning transmission electron microscopy (HAADF-STEM) and X-ray absorption spectroscopy (XAS). The obtained NiW@PtC catalyst exhibited nearly two-fold higher activity and significant improvement in stability for ORR both in rotating disk electrode (RDE) and practical fuel cell compared with undoped one. This work indicated that the Ni–W dimer sites greatly modulate the electronic structure of Pt through surface compressive strain, emphasizing the strong synergistic structure stemming from compact atomic distance, leading to great performance improvement. More importantly, combined with density function theory (DFT) calculations, the correlation between location of Ni and W atoms on Pt surface and catalytic performance was revealed from an atomic-scale perspective. These findings provide valuable insights for the rational design highly efficient Pt-based electrocatalysts modified with multiple atoms for future fuel cell applications.

Results and Discussion

The samples, including Ni–W dimer sites modified Pt nanoparticles (NPs) (denoted as NiW@PtC, shown in Figure 1a), Ni single atom modified Pt NPs (denoted as Ni@PtC) and W single atom modified Pt NPs (denoted as W@PtC) were synthesized by ALD process with commercial PtC as substrate. The deposition of Ni and W elements on the Pt NPs utilized bis(ethylcyclopentadienyl)nickel(II) and tungsten hexacarbonyl as precursors, respectively. Low magnification STEM image of NiW@PtC nanocatalysts in Figure 1b indicated that Pt NPs maintained initial morphology after the deposition of Ni and W. Furthermore, X-ray diffraction (XRD) patterns (Figure S1) and TEM images

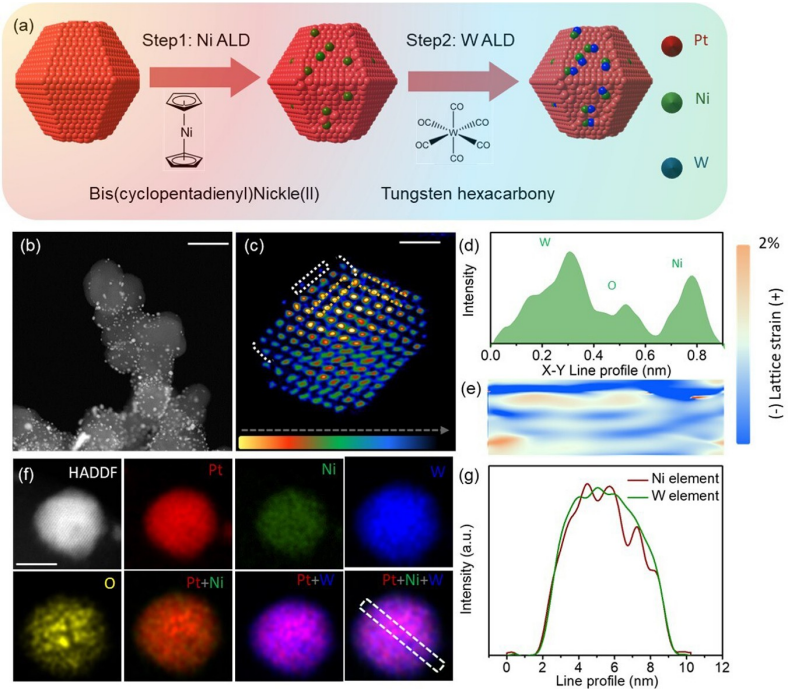

Figure 1. **(a)** Schematic illustration of the synthesis process of NiW@PtC nanocatalysts. **(b–g)** TEM characterization of NiW@PtC NPs. **(b)** Low magnification STEM image, scale bar is 50 nm. **(c)** High resolution HAADF-STEM image, scale bar is 1 nm, the gradient color bar represented the intensity (with the arrow indicating the direction from high to low). **(d)** Intensity line profile of dimer Ni–O–W obtained from white dash rectangle in Figure 1c. **(e)** Two-dimension surface strain mapping of the white dash bracket area in Figure c obtained by geometric phase analysis method. The strain scale bar is 2%, the upward direction represented the path from subsurface to outmost surface of nanoparticle in Figure 1c. **(f)** EDS elemental mapping result, scale bar is 2 nm. **(g)** Intensity of line profile of Ni and W element across the NiW@PtC nanoparticle, obtained from white dash rectangle in Figure f.

(Figure S2) confirmed that the crystal phase and particle size (approximately 3 nm) of these catalysts remained unchanged, which assumed that the deposition of single atom occurred only on the surface Pt atoms without changing the crystal structure.

To get an atomic insight into NiW@PtC NPs structure, particularly on the Ni–W dimer structure, high resolution HAADF-STEM imaging along with atomic resolution energy dispersive spectrum (EDS) analysis were further conducted. As depicted in Figure 1c, the inner structure of NiW@PtC NPs was revealed with 0.221 nm lattices spacing, which can be attributed to pure Pt(111) facet.[11] The surface structure of NiW@Pt NPs exhibited roughness with noticeable defects and steps in the atomic resolution STEM image, as indicated by white dash rectangle in the Figure 1c, suggesting the formation of densely distributed single atoms on the Pt surface. Furthermore, the surface atoms of the nanoparticle were clearly visible in the STEM images (also known as Z-contrast image), which the contrast difference depends on the atomic number and sample thickness. Consequently, the intensity line profile in Figure 1d revealed the successfully preparation of Ni–W dimers on Pt surface. More importantly, the Ni single atom and W single atom were found with an adjacent distance of 0.4 nm to each other, as shown in Figure 1d. Interestingly, one atom with weak intensity was observed between the Ni and W single atoms, which was identified as oxygen element arising from the abundance of Ni–O and W–O bonding structure in the ALD precursor. The lengths of the Ni–O and W–O bonds were approximately 2.1 Å and 1.9 Å from line profile, respectively, in accordance with previous research.[12] Besides, the high resolution STEM images of Ni@PtC and W@PtC nanoparticle, shown in Figure S3 and S4, revealed the presence of single Ni or W atoms, indicating the successful synthesis of single-atom electrocatalysts.

To investigate the impact of Ni–W dimer structure on Pt nanoparticle surface, particularly focusing on lattice distortion, two-dimension strain mapping in Figure 1e of NiW@PtC nanoparticle surface relative to pure Pt nanoparticle was performed. Figure 1e indicated that compressive strain on NiW@PtC would increase from the inner subsurface area to outermost surface region. Typically, in the surface region where the Ni–O–W dimers is located, there is a substantial compressive strain, approximately 2 %, depicted by the deep blue coloration, indicating the effective compressive strain regulation on Pt NPs surface by Ni–W dimer decoration.[13] Lattice strain, especially compressive strain in the surface generally results in a upshift of electronic structure of Pt surface atoms compared with femi level and tunes its ORR performance. Additionally, the STEM-EDS mapping results in Figure 1f showed that Ni–W dimers are uniformly dispersed on the surface of Pt NPs. The intensity of line profile from Figure 1g confirmed that Ni and W species evenly distributed across the particle surface. The composition of Ni and W with molar ratio of 3:4 and weight percent 5 % (wt%) was determined by EDS.

Complementing the atomic-scale TEM characterization, we also conducted XAS measurements to probe the electronic structure and local coordination environment of Pt element in NiW@PtC (Figure 2). The chemical state of Pt could be determined by the white line intensity (the sharp peak from the absorption edge) of Pt L_3 edge and the threshold energy E_0 in the X-ray absorption near edge spectra (XANES). Previous studies have concluded that the white line intensity is related to valence states, which can reflect the electron occupancies in the 5d orbit of transition metal element such as Pt, Ir, Au.[14] In Figure 2b, the valence state of Pt species is approximately 0.4, indicating the majority metallic and minority oxidation state of Pt in NiW@PtC.

Furthermore, the local coordination information of Pt was revealed by the extended X-ray absorption fine structure (EXAFS) and the corresponding Fourier-transformed (FT-) EXAFS R space spectra in Figure 2c. By analysis the standard reference of Pt foil and PtO_2 foil, the specific Pt–Pt bond and Pt–O bond can be found at the locations of ~2.75 Å and ~1.8 Å, respectively. In case of Pt in the NiW@PtC, the Pt–Pt bond located at 2.72 Å and a small Pt–O peak at 1.68 Å were detected, indicating the dominant metallic Pt and surface oxidized Pt species in NiW@PtC. Importantly, the shorter Pt–Pt and Pt–O bond length in NiW@PtC than those in Pt and PtO_2 foil provided evidence for the stable compressive strain, which due to Ni–W dimers modification on the Pt surface and agree well with the HAADF-STEM strain results. The coordination number and coordination species of Pt in NiW@PtC were further analyzed by fitting the EXAFS R space spectra. The results in Table S1 revealed that the NiW@PtC catalyst exhibits a relatively lower coordination number (8.7) compared to that of Pt foil (12), due to the partial Pt atomic coordination with Ni–W dimers.

Furthermore, we explored the coordination information of Ni and W elements to directly verify the single atom state and investigate local coordination structure (Figure 2d). The comparison of Ni element white line intensity showed the NiW@PtC and Ni@PtC had similar peak intensity but higher than that in Ni foil, suggesting the oxidation state of Ni atoms prepared by ALD (Figure S5). The detailed coordination information of Ni element was unveiled by the R space curves fitting results in Figure S6 and Table S2. The first peak of NiW@PtC and Ni@PtC in the R space curves was attributed to Ni–O bonds with approximately 2.05 Å, which was consistent with STEM results of 2.1 Å, further confirming that Ni species existed as single atom state. The second coordination bond at 2.55 Å was identified as Ni–Pt bonds. Additionally, similar analysis was used for obtaining W coordination configuration and electronic structure in Figure S7 and Table S3. Compared with WO_3 foil and standard W foil, the first peak in R space at 1.84 Å. was attributed to W–O bond, indicating the oxidation state and single atom configuration of W in NiW@PtC. Notably, the relatively shorter Ni–O (2.05 Å) bond length in NiW@PtC from Table S2 and S3 compared with Ni should be the strong oxygen affiliation effects from Ni–W dimer structure, inducing more compact structure and thus leading to strong synergistic effect. Figure 2e presented the wavelet-transform EXAFS analysis of Pt element from NiW@PtC, Pt and PtO_2 foil. The NiW@PtC indicated a slight shift after dimer atom

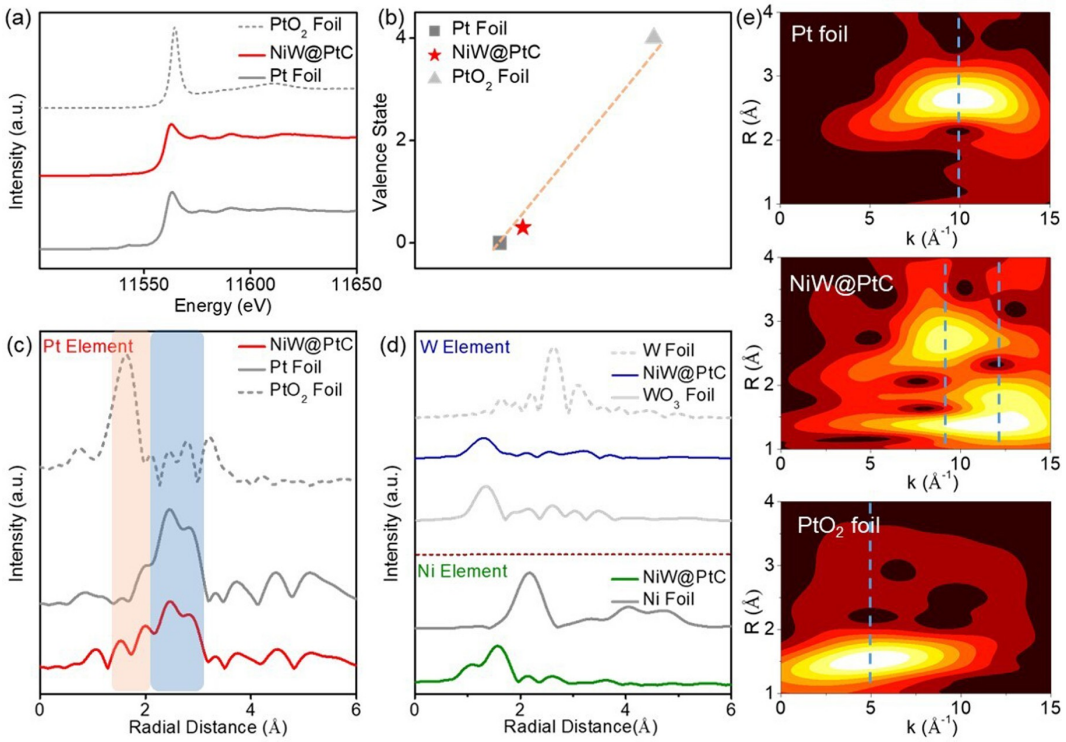

Figure 2. X-ray absorption studies of the NiW@PtC nanocatalysts in comparison with Pt and PtO_2 foil. **(a)** The normalized XANES spectra at the Pt L_3-edge of the NiW@PtC, Pt and PtO_2 foil. **(b)** The valence state analysis of Pt. **(c)** Corresponding K_3-weighted magnitude of Fourier transform spectra from EXAFS. **(d)** Corresponding K_3-weighted magnitude of Fourier transform spectra from Ni K-edge, W K-edge of NiW@PtC and corresponding reference. **(e)** WT-EXAFS spectra of Pt foil, NiW@PtC and PtO_2 foil, respectively.

deposition. Based on advanced electron microscopy and XAS analysis, we concluded that Ni and W species exist as single atom, forming tight Ni–W dimer structure that are homogeneously distributed on the Pt surface. Moreover, we revealed the valence state and coordination information of Pt species and discovered the compressive strain induced by Ni–W dimers on Pt surface, which regulated the electronic structure of Pt and achieved performance enhancement for ORR.

The ORR activity of NiW@PtC was investigated by using RDE test in the 0.1 M $HClO_4$ solution at room temperature and compared against Ni@PtC, W@PtC and commercial PtC. Before assessing catalysts' performance, an electrochemical process was used for activating and cleaning the Pt surface. Figure 3a presented the cyclic voltammogram (CV) curves of NiW@PtC and reference catalysts after dealloying process. The absorption/desorption peak on hydrogen underpotential deposition area (0.05–0.35 V) was related to the specific facet proportion of Pt NPs.[15] The similar absorption/desorption peaks of PtC and NiW@PtC suggested that the morphology remained unchanged after Ni and W species deposition. The electrochemical active surface area (ECSA) of PtC, NiW@PtC, Ni@PtC and W@PtC was calculated as 70.6, 69.1, 69.3, 61.2 $cm^2 mg_{Pt}^{-1}$, respectively. It is worth noting that the ECSA of NiW@PtC is quite close to pure PtC, highlighting that precise dimer atom decoration on Pt surface does not block the active sites of Pt. However, the W@PtC had a much lower ECSA compared with pure PtC, as well as other single/dimer atom decoration catalysts. This could be attributed to the higher density of W single atoms on the Pt surface, supported by EDS results. Additionally, Figure S8 presented the comparison of two different W composition samples and revealed that the sample with higher W content exhibited significantly lower ECSA. Figure 3b showed the ORR polarization curves of the different catalysts. It can be observed that NiW@PtC exhibited the highest ORR activity, followed by Ni@PtC and W@PtC, while PtC showed the lowest activity.

To evaluate the stability of these catalysts, especially focusing on the role of specific element, accelerated degradation tests (ADTs) were employed by conducting 4000 potential cycles between 0.6 and 1.0 V at scan rate of 100 mV/s (Figure 3c and Figure S9). The corresponding kinetic mass activity at 0.9 V before and after stability were compared in Figure 3d. Inspection of these results indicated that NiW@PtC nanocatalysts exhibited best performance both in activity (0.25 $A mg^{-1}_{Pt}$ at 0.9 V, without IR compensation) and stability (only 6 % activity loss after 4000 cycles CV). In contrast, the undoped PtC nanocatalyst showed 0.127 $A mg^{-1}_{Pt}$ mass activity and nearly 30 % loss in activity after durability test. Ni@PtC exhibited high activity (0.23 $A mg^{-1}_{Pt}$ at 0.9 V) for the ORR but its stability is compromised as it experienced a significant 40 % loss in mass activity after the durability test. On the other hand, W@PtC demonstrated higher stability with only a 13 % loss in mass activity and no enhancement in activity. These

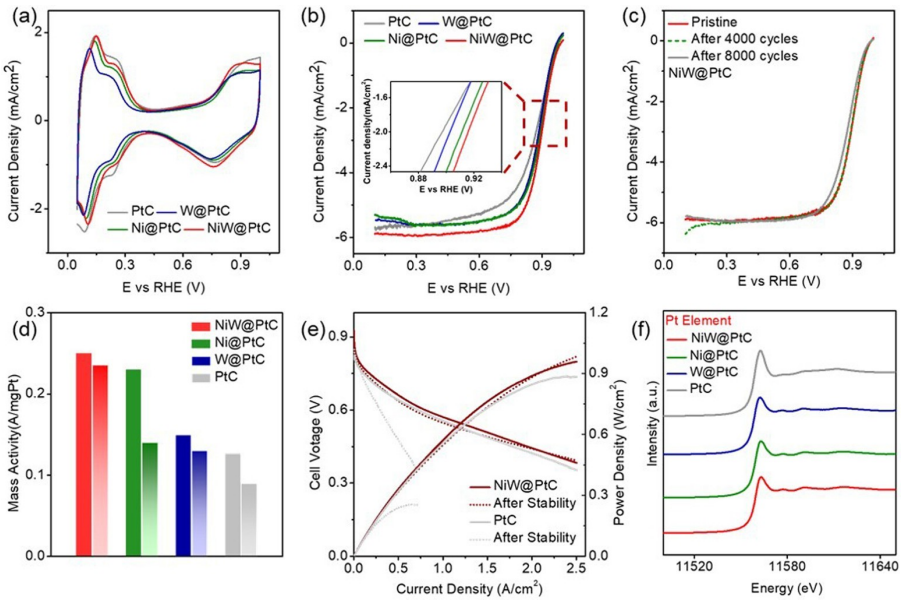

Figure 3. **(a)** The CV curves in the potential region from 0.05 to 1.0 V recorded on the NiW@PtC, Ni@PtC, W@PtC and commercial PtC. **(b)** ORR polarization curves of these catalysts. The current densities were normalized to the geometric a rea of the RDE (0.196 cm^2), the insert plot is the enlarge area of red dash rectangle. **(c)** Durability measurements of the NiW@PtC nanocatalysts. **(d)** Mass activities at 0.9 V vs RHE of four catalysts before stability (pure color) and after stability (gradient color). **(e)** H_2–O_2 fuel cell polarization curves of NiW@PtC and PtC before/after 2k stability test. Anode: 0.4 $mg_{Pt}cm^{-2}$ commercial PtC (Fuel cell store, 20%), Cathode: 0.2 $mg_{Pt}cm^{-2}$ NiW@PtC or commercial PtC. **(f)** The normalized XANES spectra at the Pt L_3-edge of the NiW@PtC, Ni@PtC, W@PtC and PtC after stability test.

results suggested that the addition of Ni greatly enhances the catalytic activity of the nanocatalysts, while the presence of W species promotes their stability. Besides, different Ni–W composition on Pt nanoparticles' ORR performance were also explored (Figure S10) and we determined that suitable composition of Ni and W is 3% and 4%, respectively. More importantly, Figure 3e presented H_2–O_2 fuel cell polarization curves and power density curves of NiW@PtC and undoped PtC. At 0.6 V, it can be found that the fuel cell with NiW@PtC cathode exhibited the current density of 0.8 $A\,cm^{-2}$, much higher than that of 0.67 $A\,cm^{-2}$ for the fuel cell composed with PtC cathode. This result indicated that NiW@PtC cathode shows better catalytic activity than PtC for the ORR in fuel cell application. Furthermore, the stability assessment in MEA revealed that after 2k CV cycles, the NiW@PtC catalysts exhibited minimal performance deterioration, whereas PtC experienced a significant decrease in activity. These findings strongly imply that the incorporation of Ni–W dimer into the PtC catalyst augments its ORR performance in both half-cell and practical fuel cell applications through synergistic effects.

To further explore the mechanism of catalytic activity difference, we compared the white line intensity peak of these catalysts, as shown in Figure 3f. The NiW@PtC exhibited the lowest white line intensity, suggesting the lowest 5d orbit unoccupied state. This result was further confirmed by the X-ray photoelectron spectroscopy (Figure S11). To quantitively investigate these catalysts' the unoccupied density of state (DOS) of 5d orbit above the fermi level, we quantitively analyzed the ratio of L_3 and L_2 of Pt edge based on reported method.[14b,16] As shown in Table S4, NiW@PtC manifested the lowest unoccupied density of state of Pt 5d orbit (0.555) compared with Ni@PtC, W@PtC. Indeed, less unoccupied density state for transition metal element such as Pt would greatly enhance its catalytic performance from previous reports.[5b,8a,17] Additionally, detailed fitting results in Figure S12 indicated the coordination number of NiW@PtC is 8.7, suggesting upshifting of d band center and more optimal reaction intermediate absorption, and thus higher ORR catalytic activity.[4,18] Additionally, to evaluate the effects of Ni–W dimer atom ORR activity, we prepared Ni–W dimer atom on carbon support with identical procedures. The ORR activity test in Figure S13 results indicated that Ni–W dimer atom had no activity for ORR and confirmed that Pt is the only active sites.

Tracking the composition and surface structure change of these catalysts before and after stability could provide valuable information on the durability. Figure 4a showed the atomic resolution STEM image of NiW@PtC after stability test. The intensity line profile in white line indicated the stable Ni–O–W dimer structure. Interestingly, we noted that the Pt atom closely sited on the dimer structure adjacent position and proposed the redeposition of Pt atoms during long term durability test (Figure 4b). To further substantiate this hypothesis, comprehensive DFT calculations were employed to illustrate that the adsorption energy of Pt atoms deposited around the Ni–O–W dimer structure (1.04 eV) is significantly lower than on the Pt surface (1.16 eV), as depicted in Figure S14. This finding suggested that the redeposition of Pt onto the Ni–O–W dimer

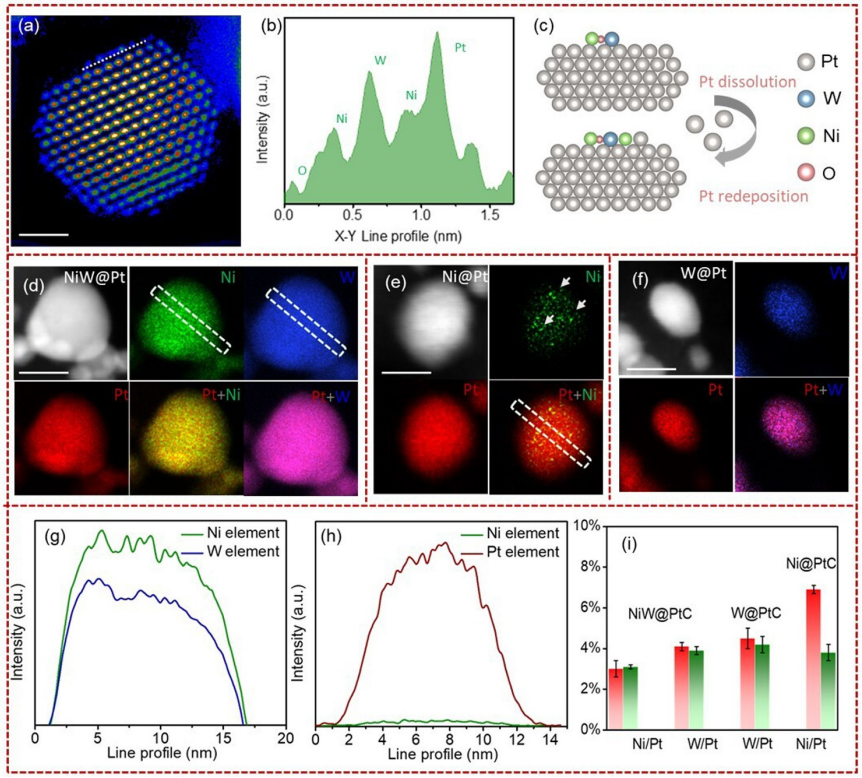

Figure 4. **(a)** High resolution STEM image of aged NiW@PtC nanoparticle, scale bar is 1 nm. **(b)** The line profile from while dash line in Figure 4a. **(c)** Model illustration of stability mechanism. **(d–f)** EDS elemental mapping of these catalysts after the stability test, scale bar is 2 nm. EDS line profiles in the elemental mapping, profile from white dash rectangle in Figure 4d–e. **(g)** NiW@PtC. **(h)** Ni@PtC. **(i)** The composition comparation of these catalysts before (red column) and after (green column) stability.

structure is very favorable, particularly under conditions of high overpotential. The morphology and elemental distribution of the aged catalysts were performed by STEM-EDS, as shown in Figure 4d–f. The Pt, Ni and W element uniformly distributed across nanoparticle and maintained its original size and morphology. However, the distribution of Ni element of Ni@PtC catalysts exhibited very weak signal when overlap with Pt species in Figure 4e. The before/after stability test particle composition of these catalysts was shown in Figure 4i. NiW@PtC maintained its pristine composition with no dissolution of Ni and only rare dissolution of W. Ni@PtC experienced severe Ni dissolution (nearly 50 % Ni dissolution) after 4000 cycles, whereas W@PtC still retained high amount of W species. The Ni dissolution is consistent with previous studies that the poor stability of PtNi alloy nanocatalysts is from fatal Ni dissolution during stability test.[10] Additionally, during the durable test, W element exhibited excellent stability with no loss after W atoms deposition. This can be attributed to the most positive standard potential W/W^{3+} (−0.09 vs RHE) and structure stability of tungsten oxide.[19] Figure 4h showed the line profile of Pt and Ni element of Ni@PtC. The peak intensity of Ni species was significantly weaker compared with Pt species after stability test. This demonstrated the role of W element in improving stability by suppressing the Ni dissolution and maintaining the pristine morphology (Figure S15) of the catalyst but Ni and W in NiW@PtC still retained its pristine composition in Figure 4g. Particularly, it is proposed that the Ni–W dimer structure plays a significant role in enhancing stability through coupling effects between Ni and W atoms.

DFT calculations were performed to study the mechanisms of high performance at the atomic level. Pt (111) was used to simulate Pt nanoparticle, and according to the HAADF-STEM images Pt atoms on Pt (111) were deposited by Ni and/or W single atoms. Furthermore, surface O atoms were added to simulate the O-containing local environments in Ni@PtC, W@PtC and NiW@PtC catalysts (Figure 5a and Figure S16). The computed free energy profile of ORR indicated that the rate-determining step (RDS) is always the O* hydrogenation to OH* and that the decoration of Ni and/or W single atom enhances the activity with the overpotential (η) of 0.65, 0.52, 0.63 and 0.47 V for Pt foil, Ni@PtC, W@PtC and NiW@PtC (Figure 5b), respectively, consistent with experimental observations (Figure 3a–b). Since surface Pt atoms are active sites for all catalysts, the projected density of states (PDOS) of active Pt sites that surround Ni and/or W single atom were analyzed (Figure 5c). The d-band center (ε) was −1.85 eV for Pt, and changed to −1.81 eV for Ni@PtC, −1.95 eV for W@PtC and −1.77 eV for NiW@PtC. The catalyst generally exhibited higher activity as the electronic states approach closer to the Fermi level.[3b,18,20]

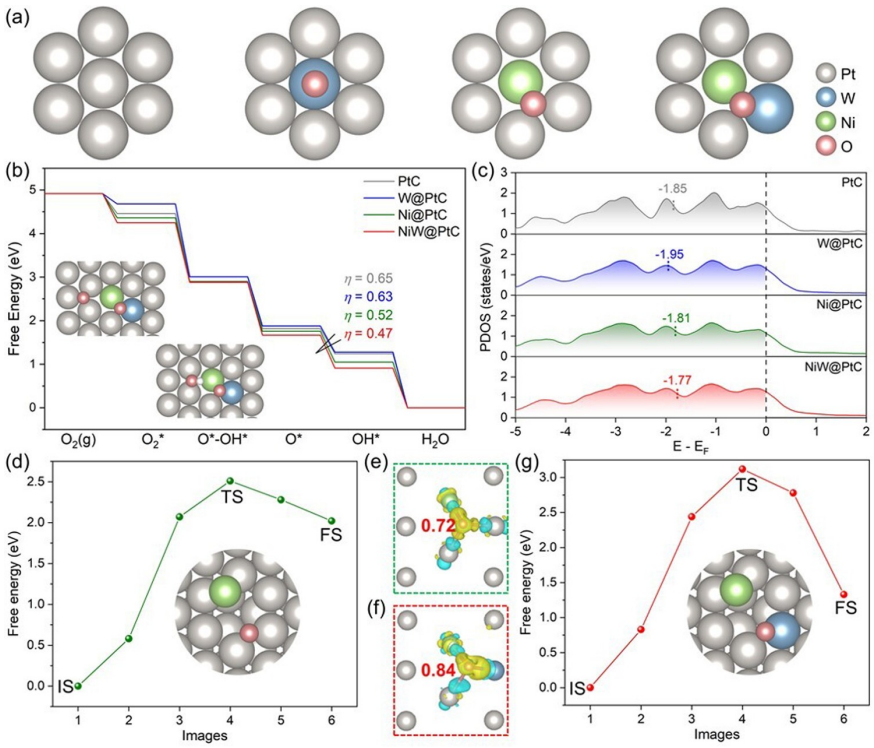

Figure 5. **(a)** Computation models in DFT investigations. **(b)** The free energy profile of ORR at the applied potential of 0 V, including the η values and the O* and OH* configurations on NiW@PtC. **(c)** PDOS of Pt-d orbitals in Pt foil, Ni@PtC, W@PtC and NiW@PtC, including the ε values. **(d)** The kinetic energy barrier of the diffusion of Ni single atom in Ni@PtC, where IS, TS and FS are initial state, transition state and final state, respectively. **(e-f)** Charge density difference plots of Ni@PtC **(e)** and NiW@PtC **(f)** with an isovalue of 0.01 $e/Å^{-3}$, where yellow and cyan regions denote electron accumulation and depletion, respectively. Red numbers are the number of obtained electrons of O atoms from the Bader charge analysis. (**g**) The kinetic energy barrier of the diffusion of Ni single atom in NiW@PtC, including the TS structure.

Activity improvement was related to the decoration of single atoms, and consequently the aggregation of single atoms to clusters/particles could lead to activity/stability degradation. Hence, the diffusion behavior of Ni single atom was studied to investigate the increased stability of NiW@PtC compared to Ni@PtC. In Ni@PtC, the kinetic diffusion barrier (E_a) of Ni single atom was 2.51 eV (Figure 5d), higher than that of Ni single atoms without O atoms (Figure S17), which demonstrated the important role of O atom in stabilizing Ni single atom. Charge density difference plots showed more electrons accumulated around the O atom after the decoration of W single atom (Figure 5e–f), suggesting the stronger O binding in NiW@PtC than Ni@PtC. The Bader charge analysis quantitively demonstrated more transferred electrons to the O atom in NiW@PtC (0.84 | e |) than Ni@PtC (0.72 | e |). The stronger O binding in NiW@PtC leaded to high barrier for Ni single atom diffusion with $E_a = 3.12$ eV (Figure 5g). Hence, Ni single atom increased the ORR activity of surface Pt sites by modulating their electronic structure, and W single atom was favorable of high stability due to its capability to enhancing the O binding, which further stabilize Ni single atoms.

Conclusion

In summary, we have successfully developed a novel high-performance electrocatalysts for ORR through the deposition of adjacent Ni and W dimer atoms on Pt surface. The as-prepared electrocatalysts exhibited two-fold activity enhancement and long-term stability in RDE and fuel cell test compared with commercial Pt/C. The aberration-corrected TEM combined with EXAFS results confirmed the successful deposition of dimer structure Ni–W on Pt surface and revealed a compressive strain of Pt surface. Additionally, XANES and XPS results revealed a less unoccupied 5d orbit density of state of Pt element after forming Ni–W dimer structure on the Pt surface, resulting from surface compressive strain, which decrease the absorption energy with oxygen intermediate and thus more favorable for ORR. Further analysis during durability tests showed that the strong synergistic Ni–W dimer structure stemming from shorten atomic distance maintained its structure, thus preserving the high catalytic performance of the NiW@PtC electrocatalysts. This work introduces a novel approach to boost Pt based electrocatalysts performance both in activity and stability by dimer atom modification, paving the way for the exploration of trimer and high entropy single atom decoration in metal nanocatalysts.

Acknowledgements

Xiaozhang Yao, Zhongxin Song and Xue Yao contributed equally to this work. This research was supported by National Natural Science Foundation of China (No. 22075203, 22279079), Guangdong Science and Technology Department Program. (2021QN02L252, 2023A1515010021), Research Team Cultivation Program of ShenZhen University (2023QNT007), Natural Sciences and Engineering Research Council of Canada (NSERC), the Canada Research Chair Program (CRC), the Canada Foundation for Innovation (CFI), Ontario Research Foundation (ORF), and the University of Western Ontario (UWO). The TEM research made use of the facilities at Canadian Centre for Electron Microscopy. The synchrotron research was performed at the Canadian Light Source, a national research facility of the University of Saskatchewan. The DFT calculations were supported by the Digital Research Alliance of Canada. We also want to acknowledge Canadian Urban Transit Research and Innovation Consortium (CUTRIC) project and Ballard Power Systems Inc.

Conflict of Interest

The authors declare no conflict of interest.

Data Availability Statement

The data that support the findings of this study are available from the corresponding author upon reasonable request.

Keywords: Dimer · Strain effects · Atomic layer deposition · Surface modification · Electrocatalytic performance

[1] a) M. K. Debe, *Nature.* **2012**, *486*, 43–51; b) H. A. Gasteiger, N. M. Markovic, *Science.* **2009**, *324*, 48–49.

[2] a) L. Gan, C. Cui, M. Heggen, F. Dionigi, S. Rudi, P. Strasser, *Science.* **2014**, *346*, 1502–1506; b) X. Huang, Z. Zhao, L. Cao, Y. Chen, E. Zhu, Z. Lin, M. Li, A. Yan, A. Zettl, Y. M. Wang, *Science.* **2015**, *348*, 1230–1234; c) Z. Wang, X. Yao, Y. Kang, L. Miao, D. Xia, L. Gan, *Adv. Funct. Mater.* **2019**, *29*, 1902987; d) R. Wang, H. Wang, F. Luo, S. Liao, *Electrochem. Energy Rev.* **2018**, *1*, 324–387; e) H. Liu, J. Zhao, X. Li, *Electrochem. Energy Rev.* **2022**, *5*, 13.

[3] a) Y. Ma, L. Miao, W. Guo, X. Yao, F. Qin, Z. Wang, H. Du, J. Li, F. Kang, L. Gan, *Chem. Mater.* **2018**, *30*, 4355–4360; b) V. R. Stamenkovic, B. S. Mun, M. Arenz, K. J. Mayrhofer, C. A. Lucas, G. Wang, P. N. Ross, N. M. Markovic, *Nat. Mater.* **2007**, *6*, 241–247; c) L. Zhang, L. T. Roling, X. Wang, M. Vara, M. Chi, J. Liu, S.-I. Choi, J. Park, J. A. Herron, Z. Xie, *Science.* **2015**, *349*, 412–416; d) M. Liu, Z. Zhao, X. Duan, Y. Huang, *Adv. Mater.* **2019**, *31*, 1802234; e) J. Greeley, I. Stephens, A. Bondarenko, T. P. Johansson, H. A. Hansen, T. Jaramillo, J. Rossmeisl, I. Chorkendorff, J. K. Nørskov, *Nat. Chem.* **2009**, *1*, 552–556.

[4] P. Strasser, S. Koh, T. Anniyev, J. Greeley, K. More, C. Yu, Z. Liu, S. Kaya, D. Nordlund, H. Ogasawara, *Nat. Chem.* **2010**, *2*, 454–460.

[5] a) M. Li, K. Duanmu, C. Wan, T. Cheng, L. Zhang, S. Dai, W. Chen, Z. Zhao, P. Li, H. Fei, *Nat. Catal.* **2019**, *2*, 495–503; b) L. Zhang, Q. Wang, L. Li, M. N. Banis, J. Li, K. Adair, Y. Sun, R. Li, Z.-J. Zhao, M. Gu, *Nano Energy* **2022**, *93*, 106813; c) L. Cao, W. Liu, Q. Luo, R. Yin, B. Wang, J. Weissenrieder, M. Soldemo, H. Yan, Y. Lin, Z. Sun, *Nature.* **2019**, *565*, 631–635; d) N. Cheng, L. Zhang, K. Doyle-Davis, X. Sun, *Electrochem. Energy Rev.* **2019**, *2*, 539–573.

[6] a) L. Bai, C.-S. Hsu, D. T. Alexander, H. M. Chen, X. Hu, *Nat. Energy.* **2021**, *6*, 1054–1066; b) L. Zhang, R. Si, H. Liu, N. Chen, Q. Wang, K. Adair, Z. Wang, J. Chen, Z. Song, J. Li, *Nat. Commun.* **2019**, *10*, 4936; c) Y. Yang, Y. Qian, H. Li, Z. Zhang, Y. Mu, D. Do, B. Zhou, J. Dong, W. Yan, Y. Qin, *Sci. Adv.* **2020**, *6*, 6586.

[7] a) J. Wang, W. Liu, G. Luo, Z. Li, C. Zhao, H. Zhang, M. Zhu, Q. Xu, X. Wang, C. Zhao, *Energy Environ. Sci.* **2018**, *11*, 3375–3379; b) Z. Lu, B. Wang, Y. Hu, W. Liu, Y. Zhao, R. Yang, Z. Li, J. Luo, B. Chi, Z. Jiang, *Angew. Chem. Int. Ed.* **2019**, *131*, 2648–2652; c) W. Ren, X. Tan, W. Yang, C. Jia, S. Xu, K. Wang, S. C. Smith, C. Zhao, *Angew. Chem. Int. Ed.* **2019**, *58*, 6972–6976.

[8] a) N. Cheng, S. Stambula, D. Wang, M. N. Banis, J. Liu, A. Riese, B. Xiao, R. Li, T.-K. Sham, L.-M. Liu, *Nat. Commun.* **2016**, *7*, 13638; b) H. Yan, Y. Lin, H. Wu, W. Zhang, Z. Sun, H. Cheng, W. Liu, C. Wang, J. Li, X. Huang, *Nat. Commun.* **2017**, *8*, 1070; c) J. Gu, M. Jian, L. Huang, Z. Sun, A. Li, Y. Pan, J. Yang, W. Wen, W. Zhou, Y. Lin, *Nat. Nanotechnol.* **2021**, *16*, 1141–1149; d) J. Li, Y.-f. Jiang, Q. Wang, C.-Q. Xu, D. Wu, M. N. Banis, K. R. Adair, K. Doyle-Davis, D. M. Meira, Y. Z. Finfrock, *Nat. Commun.* **2021**, *12*, 6806.

[9] a) L. Gao, Z. Yang, T. Sun, X. Tan, W. Lai, M. Li, J. Kim, Y. F. Lu, S. I. Choi, W. Zhang, *Adv. Energy Mater.* **2022**, *12*, 2103943; b) D. Kobayashi, H. Kobayashi, D. Wu, S. Okazoe, K. Kusada, T. Yamamoto, T. Toriyama, S. Matsumura, S. Kawaguchi, Y. Kubota, *J. Am. Chem. Soc.* **2020**, *142*, 17250–17254.

[10] C. Cui, L. Gan, M. Heggen, S. Rudi, P. Strasser, *Nat. Mater.* **2013**, *12*, 765–771.

[11] X. Yao, Y. Wei, Z. Wang, L. Gan, *ACS Catal.* **2020**, *10*, 7381–7388.

[12] Q. Zhao, J. Wang, Y. Cui, X. Ai, Z. Chen, C. Cao, F. Xu, Y. Gao, *Mater Adv* **2021**, *2*, 4667–4676.

[13] a) L. Bu, N. Zhang, S. Guo, X. Zhang, J. Li, J. Yao, T. Wu, G. Lu, J.-Y. Ma, D. Su, *Science.* **2016**, *354*, 1410–1414; b) M. Luo, S. Guo, *Nat. Rev. Mater.* **2017**, *2*, 1–13.

[14] a) D. Pearson, C. Ahn, B. Fultz, *Phys. Rev. B.* **1993**, *47*, 8471; b) D. Wang, X. Cui, Q. Xiao, Y. Hu, Z. Wang, Y. Yiu, T. Sham, *AIP Adv.* **2018**, *8*.

[15] H. A. Gasteiger, S. S. Kocha, B. Sompalli, F. T. Wagner, *Appl. Catal. B* **2005**, *56*, 9–35.

[16] T. Sham, S. Naftel, I. Coulthard, *J. Appl. Phys.* **1996**, *79*, 7134–7138.

[17] P. Hu, Z. Huang, Z. Amghouz, M. Makkee, F. Xu, F. Kapteijn, A. Dikhtiarenko, Y. Chen, X. Gu, X. Tang, *Angew. Chem. Int. Ed.* **2014**, *53*, 3418–3421.

[18] A. Kulkarni, S. Siahrostami, A. Patel, J. K. Nørskov, *Chem. Rev.* **2018**, *118*, 2302–2312.

[19] J. Liang, N. Li, Z. Zhao, L. Ma, X. Wang, S. Li, X. Liu, T. Wang, Y. Du, G. Lu, *Angew. Chem. Int. Ed.* **2019**, *58*, 15471–15477.

[20] V. Stamenkovic, B. S. Mun, K. J. Mayrhofer, P. N. Ross, N. M. Markovic, J. Rossmeisl, J. Greeley, J. K. Nørskov, *Angew. Chem. Int. Ed.* **2006**, *45*, 2897–2901.

Manuscript received: December 7, 2023
Accepted manuscript online: March 19, 2024
Version of record online: April 16, 2024